Whole Wheat Flour Hydrolysate Modified Urea-Formaldehyde Resin with Enhanced Wet-State Bonding Performance

Zheng Liu,[a] Chengkang Wu,[a] Shaomeng Song,[a] Weixing Gan,[a,b]* and Hailin Mo [a,c]*

* *Corresponding authors: Weixing Gan, gwxgxdx@126.com; Hailin Mo, mohailinok@qq.com*

DOI: 10.15376/biores.21.4.11562-11580

GRAPHICAL ABSTRACT

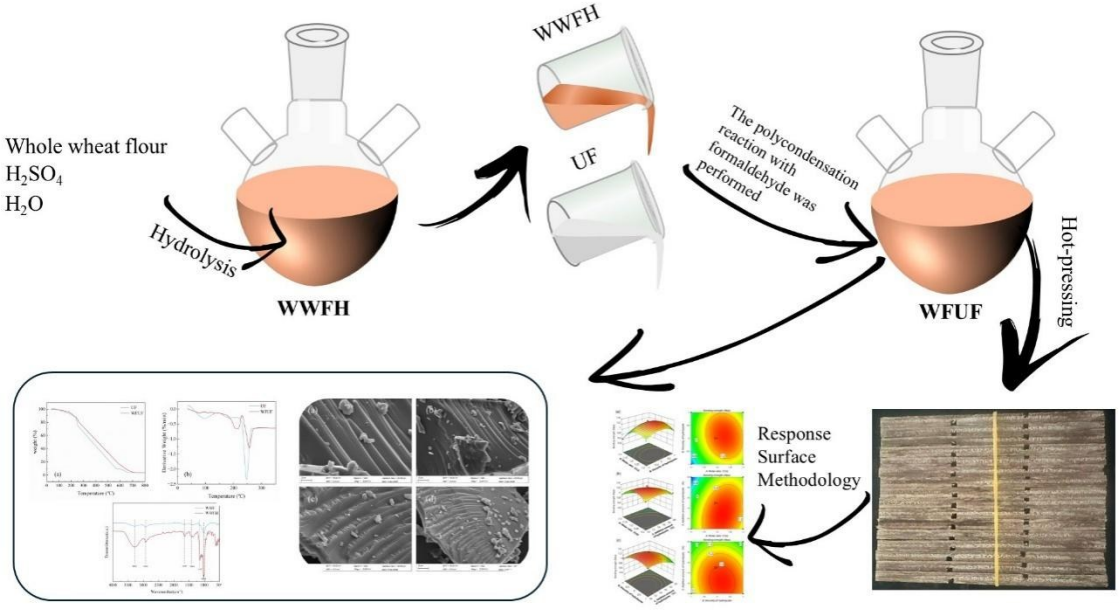

Whole Wheat Flour Hydrolysate Modified Urea-Formaldehyde Resin with Enhanced Wet-State Bonding Performance

Zheng Liu,[a] Chengkang Wu,[a] Shaomeng Song,[a] Weixing Gan,[a,b,*] and Hailin Mo [a,c,*]

Urea-formaldehyde (UF) resin is widely used in wood-based panels due to low cost and fast curing, but its high brittleness, low wet strength, and formaldehyde emissions restrict outdoor and high-humidity applications. Traditional biomass modifiers (starch, cellulose, or lignin) rely on hydrogen bonding or simple condensation with UF, offering limited improvement in wet-state bonding strength and stress distribution. This study used industrial-grade whole wheat flour to prepare hydrolysate (WWFH) *via* acid-catalyzed hydrolysis and optimized the co-condensation with UF resin by response surface methodology. The optimized wheat flour–based UF (WFUF) showed wet shear strength of 1.30 MPa (54.8% higher than 0.84 MPa for neat UF) and dry shear strength of 1.66 MPa. Formaldehyde emission was 0.59 mg/L, meeting the E1 standard. Characterization indicated that WWFH reducing sugars, protein degradation products, and pentosans crosslinked into the cured network through hydroxymethylation, urea linkages, and ether bonds. WFUF exhibited lower crystallinity, higher crosslinking density, and better thermal stability than neat UF. This work supports value-added use of low-cost whole wheat flour and development of high-performance biomass-modified UF resins.

DOI: 10.15376/biores.21.4.11562-11580

Keywords: Lignocellulose-based adhesive; Whole wheat flour hydrolysate; Urea-formaldehyde resin; Biomass modification; Bonding strength

Contact information: a: College of Environment and Resources, Guangxi Normal University, Guilin 541000, China; b: School of Resources, Environment and Materials, Guangxi University, Nanning 530004, China; c: Resource county Tiansheng New Material Development Co., Ltd, Guilin 541400, China;
** Corresponding authors: Weixing Gan, gwxgxdx@126.com; Hailin Mo, mohailinok@qq.com*

INTRODUCTION

While modification of UF resin (Dunky 1998; Dorieh *et al*. 2022) with single biomass components—such as starch, cellulose, lignin, and agricultural wastes—has been extensively investigated (Wang *et al*. 2017; Gao *et al*. 2020; Park and Park 2021; Li *et al*. 2023; Dhawale *et al*. 2022; Tian *et al*. 2023), notable limitations persist. Starch can improve toughness but shows poor interfacial compatibility with the UF matrix, and excessive loading causes a sharp rise in viscosity (Wang *et al*. 2017; Kawalerczyk *et al*. 2019; Wibowo and Park 2024; Calvez *et al*. 2024). Cellulose and its derivatives enhance mechanical properties to some extent (Antov *et al*. 2021; Park and Park 2021), yet their low reactivity limits effective covalent crosslinking (Fritz and Olivera 2022; Tian *et al*. 2023; Poschiavo *et al*. 2025).

Lignin offers high thermal stability but suffers from low reactivity and considerable steric hindrance, which restricts its substitution level and compromises batch-to-batch consistency (Gao *et al*. 2020; Li *et al*. 2023). Such single-component modifications mainly rely on physical blending or weak hydrogen bonding (Ma *et al*. 2022; Xu *et al*. 2022), rather than forming stable covalent crosslinking networks with UF resin. As a result, the improvement in wet-state bonding strength remains insufficient (Khorramabadi *et al*. 2023; Kong *et al*. 2023; Yang *et al*. 2023), and the reduction in formaldehyde emission is not significant (Hogger *et al*. 2021; Saito *et al*. 2021; Dorieh *et al*. 2022; Sandahl *et al*. 2022). These limitations arise from the absence of multi-component combined effects. Thus, there is still a bottleneck in performance gains, which highlights the need for alternative modification strategies (Hussin *et al.* 2022; Kumar and Leggate 2022).

Whole wheat flour (Kawalerczyk *et al*. 2019; Wibowo and Park 2024; Zhang *et al*. 2025) comprises multiple constituents, including starch, protein, and non-starch polysaccharides. It can be used directly without separation or purification. It offers low raw material costs and a stable supply. Acid-catalyzed hydrolysis (Ma *et al*. 2022; Pu *et al*. 2022) cleaves the macromolecular chains in whole wheat flour, exposing active sites such as hydroxyl, amino, and phenolic hydroxyl groups that can engage in multiple crosslinking reactions (Gao *et al*. 2020; Moutousidis *et al*. 2023) with UF prepolymers to build a dense, water-resistant network. To date, research on the multi-component combined modification of UF resin with whole wheat flour remains scarce (Kawalerczyk *et al*. 2019; Wibowo and Park 2024; Zhang *et al*. 2025), and the interaction mechanisms among its constituents as well as the evolution patterns of the cross-linked structure are still poorly understood.

Accordingly, this study employed industrial-grade whole wheat flour (WWF) as feedstock to prepare an acid hydrolysate and optimize its co-polycondensation with UF resin. The bonding performance, formaldehyde emission, and structural characteristics of the modified resin were systematically evaluated to elucidate the multi-component cross-linking interaction mechanism, thereby providing a scientific basis for the value-added utilization of low-cost whole wheat flour and the development of bio-based UF resins (Hussin *et al*. 2022; Kumar and Leggate 2022; Xu *et al*. 2024).

EXPERIMENTAL

Materials

All chemicals used in the experiments, including formaldehyde (37 wt % aqueous solution), urea (≥99.0%), sulfuric acid （98 wt %, formic acid （88 wt %, ammonium chloride （≥99.5%, and sodium hydroxide （≥96%, were of analytical grade and purchased from Xilong Scientific Co. Ltd. (Guangdong, China). The whole wheat flour (feed grade) used in this study had a typical composition as follows: crude protein 10 to 15%, starch 52 to 60%, total sugars 2 to 11%, crude fat 1.5 to 2.5%, dietary fiber 6 to 8%, and moisture ≤ 14%). It was supplied by Mengcheng Tianyi Flour Industry Co. Ltd. (Anhui, China), Whole wheat flour (food grade) was obtained from Guoyang County Xuelian Flour Co., Ltd., and eucalyptus veneers (480 mm × 480 mm × 1.7 mm, moisture content 8% to 12%, with an air-dried density of 0.59 g/cm³, and without insect damage, cracks, or knots.) were provided by Guilin Wood Factory (Guangxi, China).

Process Flow Diagram

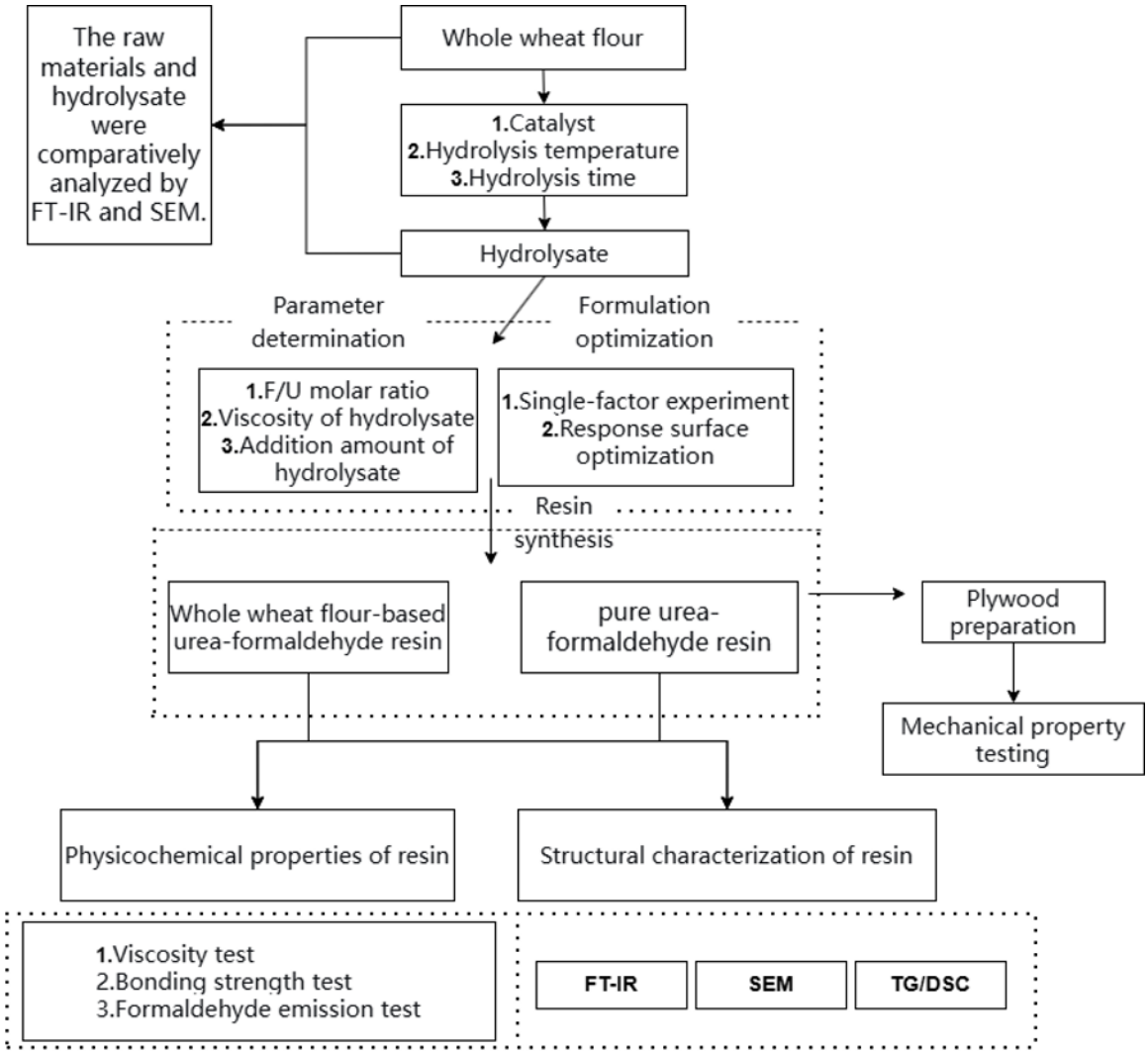

Fig. 1. Process flow diagram

Preparation of Whole Wheat Flour Hydrolysate

Concentrated sulfuric acid was diluted and added at 6 wt% (based on the whole wheat flour mass) into a four-necked flask equipped with a reflux condenser. The flask was placed in a 60 °C water bath with stirring, and whole wheat flour was then added. The reaction was continued until the hydrolysate viscosity reached 20 to 40 s as measured with a Ford Cup No. 4 at 30 °C according to GB/T 1723 (1993), corresponding to approximately 0.70-1.41 poise. After cooling, the pH was adjusted to 7 using 40% NaOH solution to obtain whole wheat flour hydrolysate (WWFH).

Synthesis of Pure UF Resin

Formaldehyde solution (324 g) was added to a four-necked flask, and the pH was adjusted to the range 8 to 9 with 40 wt % NaOH solution. The first batch of urea (112 g) was added and reacted at 90 °C for 40 min. The pH was then adjusted to 4.5 to 5.5 with 40% formic acid solution, and the reaction was continued at 90 °C until the viscosity reached 23 to 28 s (measured with a Ford Cup No. 4). The pH was readjusted to 7 with

40% NaOH solution, and the second batch of urea (44 g) was added and reacted at 85 °C for 30 min. The temperature then lowered to 60 °C. Finally, the third batch of urea (44 g) was added and reacted at 60 °C for 40 min, after which the mixture was cooled to 30 °C to yield a transparent UF resin.

Synthesis of Whole Wheat Flour–Based UF (WFUF) Resin

Formaldehyde solution (324 g) was added to a four-necked flask. After adjusting the pH to 8 to 9 with 40 wt % NaOH solution, the first batch of urea (112 g), and 92.5 g of WWFH were added and reacted at 90 °C for 40 min. Subsequent steps followed the same procedure as for the pure UF resin, yielding the whole wheat flour–based UF (WFUF) resin.

Preparation of Three-Ply Plywood and Bonding Strength Testing

High-quality eucalyptus veneers were used as the core layer. Adhesive was applied manually at a spread level of 168 g/m² (single-sided), and the veneers were assembled with perpendicular grain orientation. The assembly was first cold-pressed at room temperature for 40 min, then hot-pressed at 115 °C and 1.2 MPa for 480 s.

In accordance with GB/T 17657 (2022) standard, the plywood was cut into specimens measuring 100 mm × 25 mm. Grooves were cut on both sides of each specimen to a depth of approximately 2/3 of the panel thickness, creating a bonded area of 25 mm × 25 mm. The specimens were then immersed in hot water at 63 °C for 3 h, followed by drying at room temperature (25 ± 3 °C) for 20 min. The wet shear strength was measured using a universal testing machine (MWW-10A, Jinan Xinguang Testing Machine Manufacturing Co., Ltd., Jinan, China) with a cross-head speed of 2 mm·min^{-1}. At least 10 specimens per batch were tested to calculate the average value, and the wet and dry strength data of the hot-pressed panels were also recorded.

Formaldehyde Emission Measurement

The formaldehyde emission was determined by the desiccator method specified in GB/T 17657 (2022). Specimens were conditioned at 23 ± 1 °C and 50 ± 5% relative humidity for 7 days, then placed in a desiccator at 25 ± 1 °C for 24 h with 300 mL of distilled water added. After 24 h, 25 mL of the absorption solution was transferred to a conical flask, mixed with 5 mL of acetylacetone–ammonium acetate color-developing reagent (prepared by dissolving 150 g of ammonium acetate (≥98.0%, analytical grade) in approximately 800 mL of distilled water, followed by the addition of 3 mL of glacial acetic acid (analytical grade) and 2 mL of acetylacetone (99%, analytical grade), with thorough stirring and dilution to 1 L with distilled water), and color-developed in a 65 °C water bath (Shao *et al*. 2022). Absorbance was measured using a UV spectrophotometer (M/VOC1200, Munee Test Experiment (Shanghai) Co., Ltd., Shanghai, China) at a wavelength of 412 nm.

$$C = f \times (A_s - A_b) \times \frac{1800}{A} \quad (1)$$

where C is the formaldehyde mass concentration (mg/L), f is the slope of the formaldehyde standard curve (mg/L), A_s is the absorbance of the test solution, A_b is the absorbance of the blank control, and A is the specimen surface area (cm²).

Fourier Transform Infrared Spectroscopy

Approximately 10 to 12 mg of sample was weighed, freeze-dried at −70 °C for 16 h, and then vacuum-dried for 24 h. The dried sample was mixed with 500 mg of dried KBr and pressed into a pellet under 15 MPa pressure. Fourier transform infrared (FT-IR) spectra were recorded using an FT-IR spectrometer (Spectrum Two, Perkin-Elmer, Waltham, USA) equipped with a high-sensitivity diamond crystal, over a scanning range of 400 to 4000 cm^{-1}, with a resolution of 4 cm^{-1} and 64 cumulative scans (Gao *et al*. 2020; Xu *et al*. 2022).

Scanning Electron Microscopy

The sample was treated at −70 °C for 24 h and then ground into powder. The powder was evenly sprinkled onto conductive adhesive tape, and the surface was sputter-coated with gold to enhance conductivity. Micro-morphology was observed using a field-emission scanning electron microscope (Zeiss Sigma 300, Carl Zeiss AG, Oberkochen, Germany) (Dukarska *et al*. 2024; Psochia *et al*. 2025).

Thermogravimetric Analysis

Thermal stability (Gao *et al*. 2020; Antov *et al*. 2021; Ma *et al*. 2022) of UF and WFUF resins was determined using a thermogravimetric (TG) analyzer. Nitrogen was used as the carrier gas at a flow rate of 20 mL/min, with a heating rate of 20 K/min over a temperature range of 30 to 900 °C. The sample mass of 8 to 10 mg, placed in an aluminum crucible, pre-treated at 120 °C for 2 h, and then ground into powder.

Single-Factor Experimental Design

Based on pre-test conditions (sulfuric acid at 6 wt% relative to the whole wheat flour mass, with reaction time varied to obtain hydrolysates in different viscosity ranges), bonding strength and storage time were used as reference indices to investigate the effect of hydrolysate viscosity range on the bonding strength of UF resin. While maintaining constant masses of whole wheat flour, sulfuric acid, and pure water, the influence of hydrolysate viscosity ranges—below 20 s, 21 to 30 s, 31 to 40 s, 41 to 50 s, 51 s to 1 min, and above 1.0 min (measured with a Ford Cup No. 4)—on the bonding strength and storage time of the resulting UF resin was evaluated. The results indicated that when the hydrolysate viscosity fell within the ranges of 21 to 30 s, 31 to 40 s, and 41 to 50 s, the bonding strength of the UF resin was significantly enhanced, and the synthesized UF resin could be stored for more than 30 days.

Box–Behnken Response Surface Methodology for Experimental Design

Response surface methodology (RSM) is an effective experimental approach capable of reflecting interactions among factors and identifying optimal process parameters. In this study, bonding strength was selected as the response value. A response surface experimental design for WFUF resin was established with the molar ratio of UF resin (A), hydrolysate viscosity (B), and hydrolysate addition amount (C) as independent variables.

The Box–Behnken response surface method in Design-Expert 13 software was employed for data fitting and analysis to determine the optimized process parameters. The factors and their levels are presented in Table 1.

Table 1. Factor Level Design

Level	Molar ratio, A (F/U)	Hydrolysate Viscosity, B (s)	Hydrolysate Addition Amount, C (%)
−1	1.1	21 to 30	10
0	1.2	31 to 40	15
1	1.3	41 to 50	20

RESULTS AND DISCUSSION

Single-Factor Experimental Design

Response-surface methodology was adopted to optimize the co-polycondensation parameters of WFUF resin and evaluate its plywood bonding performance. According to the experimental design, a Box–Behnken fitting model was established for the experimental data using Design-Expert 13 software; the results are shown in Table 4. A total of 17 experimental runs were conducted, comprising 12 factorial runs and 5 center points for evaluating experimental error.

The data in Table 2 were analyzed to establish a mathematical model, yielding the following quadratic regression Eq. 2:

$$Y=1.30+0.152\ 5\times A+0.050\ 0\times B-0.125\ 0\times C-0.060\ 0\times AB+0.095\ 0\times AC-0.030\ 0\times BC-0.257\ 0\times A^2-0.172\ 0\times B^2-0.122\ 0\times C^2 \quad (2)$$

Table 2. Response Surface Test Design Scheme and Results

Run No.	Molar Ratio, A (F/U)	Hydrolysate Viscosity, B (s)	Hydrolysate Addition Amount, C (%)	Bonding Strength, Y(MPa)
1	0	1	1	0.87
2	0	0	0	1.26
3	0	0	0	1.34
4	0	-1	-1	1.09
5	0	0	0	1.36
6	-1	0	1	0.54
7	1	1	0	1.00
8	-1	-1	0	0.63
9	-1	1	0	0.88
10	0	0	0	1.27
11	1	-1	0	0.99
12	0	0	0	1.29
13	1	0	1	1.10
14	1	0	-1	1.12
15	-1	0	-1	0.94
16	0	-1	1	0.86
17	0	1	-1	1.22

** The symbols -1, 0, and 1 in columns B and C represent coded levels corresponding to the actual values listed in Table 1. Specifically, for hydrolysate viscosity (B): -1 = 21–30 s, 0 = 31–40 s, 1 = 41–50 s; for hydrolysate addition amount (C): -1 = 10%, 0 = 15%, 1 = 20%. Each run number corresponds to a different experimental condition generated by the Box-Behnken design for response surface optimization.*

Analysis of Variance for the Regression Model

Design-Expert 13 software was used to establish a Box–Behnken fitting model for the experimental data. On this basis, analysis of variance and comparison of the mathematical models yielded the results presented in Table 5. According to the ANOVA for the regression model in Table 3, the model F-value was 33.02 and the P-value was <0.0001, indicating that the model was extremely significant. The lack-of-fit F-value was 2.32 with a P-value of 0.2166, indicating that lack of fit was not significant. The extremely significant P-value of the model ($P < 0.0001$) and the non-significant lack-of-fit as indicated by F-value ($P = 0.2166 > 0.05$) demonstrate that the quadratic regression model established by response surface methodology exhibited good fitness. R^2 was used to represent the fitting degree of the quadratic regression equation; an R^2 greater than 0.8 is generally considered to indicate good fitness. As shown in Table 3, R^2 was 0.9770 in this experiment, indicating a high correlation between the model and actual conditions. The adjusted coefficient of determination (Adjusted R^2) was 0.9474, and the adequate precision (signal-to-noise ratio) was 17.8173 (adequate precision > 4), demonstrating high model reliability and confirming that the fitness of the quadratic regression equation was highly dependable. Additionally, as shown in Fig. 2, in the normal probability plot and the predicted *vs*. actual plot, the points for predicted and actual values fell approximately on the straight line; in the residuals *vs*. predicted plot, the data points were randomly distributed, indicating a high correlation between predicted and actual values under normal probability, demonstrating that the variable functions conformed to a normal distribution and that experimental values were similar to predicted values obtained from the fitted model. Therefore, the data were reliable, and the predicted optimal value was in complete agreement with the experimental optimal value.

To further examine the established model, significance analysis of the equation was performed; the results are shown in Table 3. The linear term A ($P < 0.0001$) exhibited extremely significant difference, the linear term B ($P = 0.0369$) exhibited significant difference, the linear term C ($P = 0.0004 < 0.01$) exhibited highly significant difference, A^2 ($P < 0.0001$) exhibited extremely significant difference, B^2 ($P = 0.0004 < 0.01$) exhibited highly significant difference, and C^2 ($P = 0.0026 < 0.05$) exhibited significant difference. According to F-value analysis, the order of influence of the three factors on bonding strength was molar ratio > hydrolysate addition amount > hydrolysate viscosity. In summary, this model exhibits high fitness with small experimental error, can describe the true relationships between various factors and the response value, and can be used to analyze and predict the optimal preparation process for whole wheat flour–based UF resin.

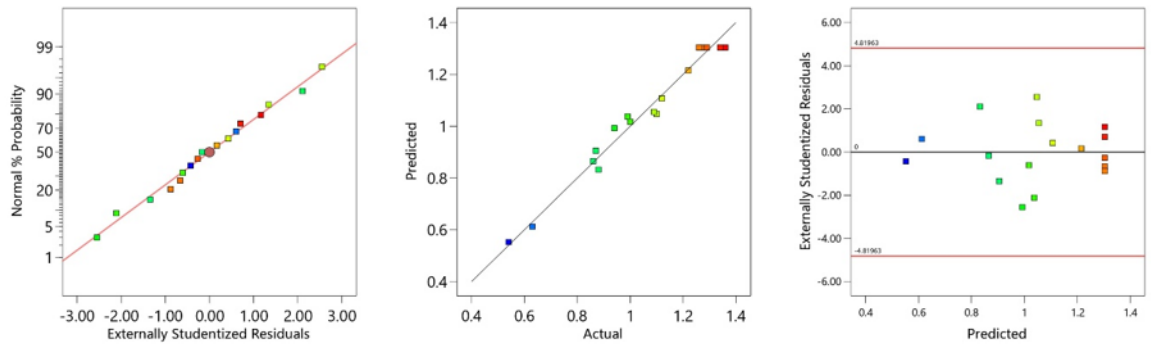

Fig. 2. Plot of normal probability distribution predicted *versus* actual values of gluing strength, and residual prediction

Table 3. Regression Model Analysis of Variance

Source	Sum of Squares	df	Mean Square	F-value	P-value	
Model	0.8987	9	0.0999	33.02	<0.001	Significant
A	0.1861	1	0.1861	61.52	0.001	
B	0.0200	1	0.0200	6.61	0.0369	
C	0.1250	1	0.1250	41.33	0.0004	
AB	0.0144	1	0.0144	4.76	0.0654	
AC	0.0361	1	0.0361	11.94	0.0106	
BC	0.0036	1	0.0036	1.19	0.3114	
A^2	0.2781	1	0.2781	91.96	<0.0001	
B^2	0.1246	1	0.1246	41.19	0.0004	
C^2	0.0627	1	0.0627	20.72	0.0026	
Residual	0.0212	7	0.0030			
Lack of Fit	0.0134	3	0.0045	2.32	0.2166	Not Significant
Pure Error	0.0077	4	0.0019			
Cor Total	0.9198	16				
Std. Dev.	0.0550		R^2	0.9770		
Mean	1.04		Adjusted R^2	0.9474		
C.V. %	5.26		Predicted R^2	0.7529		
Adeq. Precision	17.8173					

Response Surface Analysis

Based on the established model, three-dimensional response surface plots and two-dimensional contour plots were generated for the remaining two factors while holding one factor at its zero (center) level. The response surface plots illustrate the effects of the variables on the bonding strength of WFUF resin. When the contour lines approach an elliptical shape, this indicates relatively strong interaction significance between the two factors; in the three-dimensional response surface plots, the more pronounced the curvature, the greater the effect of the investigated factor on the result, and *vice versa*. As shown in Fig. 3, the response surfaces were convex in shape, with both the center and edge points falling within the investigated range, indicating the presence of an optimal response for the bonding strength of WFUF resin. Figure 3(a) shows the effects of the UF resin molar ratio and hydrolysate viscosity on bonding strength under fixed hydrolysate addition conditions. The curve for the UF resin molar ratio was more steeply curved, and the contour lines between the molar ratio and hydrolysate viscosity exhibited an elliptical shape. The response surface for the UF resin molar ratio showed a steeper slope, indicating that the molar ratio exerted a more significant effect. As shown in Fig. 3(b), under fixed hydrolysate viscosity, the curve for the UF resin molar ratio in the three-dimensional response surface plot was more steeply curved, and the two-dimensional contour plot showed an elliptical pattern, indicating that the UF resin molar ratio had a more significant effect on bonding strength than the hydrolysate addition amount. As shown in Fig. 3(c), under fixed UF resin molar ratio, the curve for the hydrolysate addition amount in the three-dimensional response surface plot was more steeply curved than that for hydrolysate viscosity, and the two-dimensional contour plot exhibited an elliptical shape, indicating that the hydrolysate additional amount had a more significant effect on bonding strength than the hydrolysate viscosity.

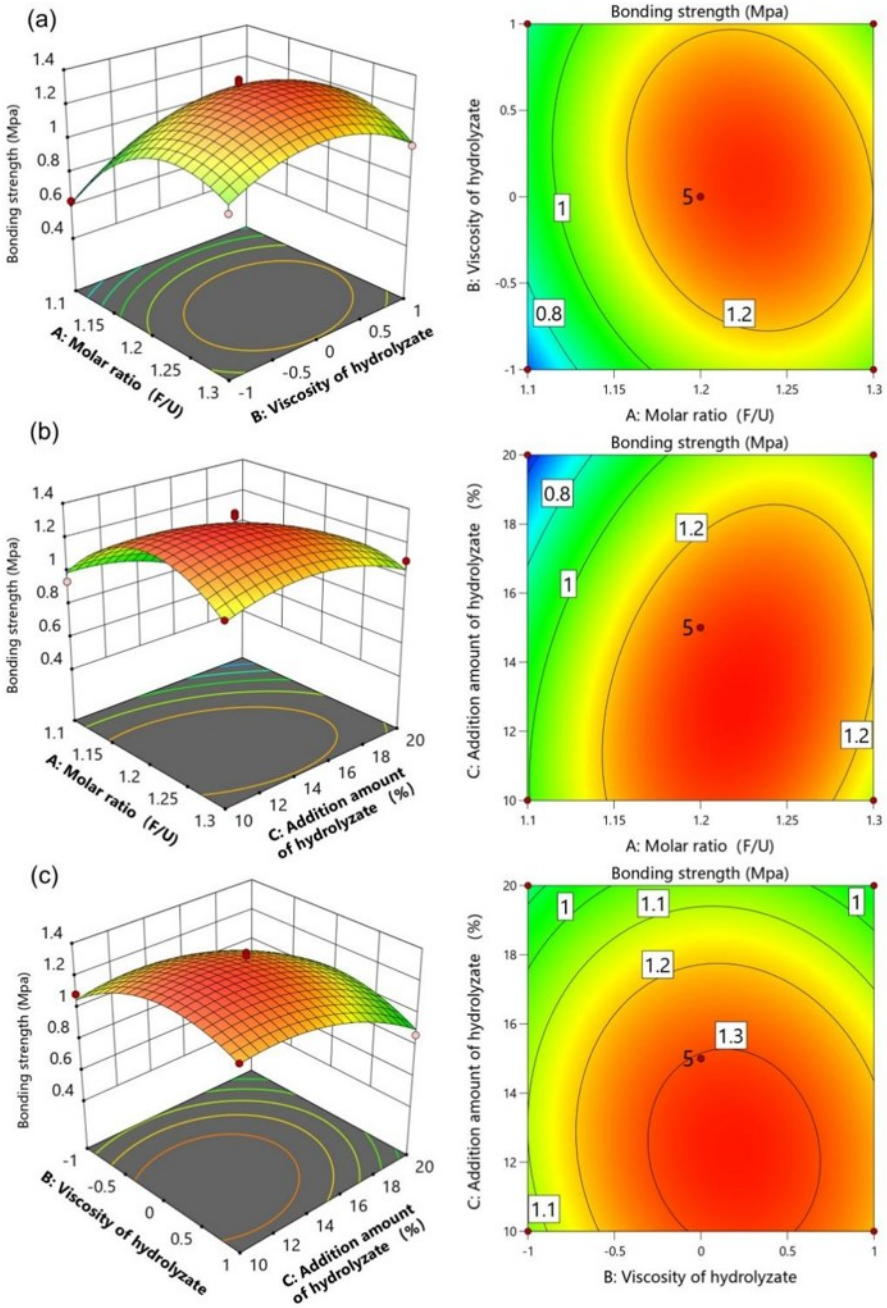

Fig. 3. Response surface interaction plot: (a) Interaction between molar ratio and hydrolysate viscosity; (b) Interaction between molar ratio and hydrolysate addition amount; and (c) Interaction between hydrolysate viscosity and hydrolysate addition amount

The extremely significant effect of the F/U molar ratio on bonding strength ($P < 0.0001$) is consistent with previous reports that the molar ratio governs the content of methylol groups in UF prepolymers, which directly affects crosslinking density and mechanical performance (Song *et al.* 2025; Ma *et al.* 2022). Statistical results demonstrate that hydrolysate dosage imposes a significant influence on bonding strength. This trend can be explained from the perspective of resin cross-linking and functional-group reactions. Within an appropriate dosage range, active components derived from wheat-flour

hydrolysate can participate in the polycondensation reaction of urea-formaldehyde resin, optimizing the cross-linking network structure and improving bonding performance. Nevertheless, excessive hydrolysate will dilute the effective reactive groups of the UF system. A large amount of non-reactive small-molecule substances introduced by hydrolysate hinder the curing cross-linking process, which finally leads to the decline of bonding strength.

Formaldehyde Emission of WFUF Resin

The formaldehyde emission of the WFUF resin prepared under the optimized conditions (F/U molar ratio of 1.2, WWFH viscosity of 31 to 40 s, and hydrolysate addition amount of 15%), as determined by the desiccator method according to GB/T 17657 (2022), was 0.59 mg/L. Although slightly higher than that of neat UF resin (0.51 mg/L), this value is far below the E1 grade limit of 1.5 mg/L specified in GB 18580–2017, confirming that the WFUF resin still meets the environmental requirement for indoor-use wood-based panels. The slight increase in formaldehyde emission can be attributed to the abundant hydroxyl and amino groups present in the WWFH. If these reactive groups are not fully consumed during the crosslinking reaction, they may form new oxygen-containing structures that could partially decompose and release formaldehyde under certain conditions.

FT-IR Analysis

FT-IR spectroscopy was performed to characterize the chemical structural variations of raw flour, hydrolysate, neat UF and modified WFUF resin. As shown in Fig. 4, the FT-IR spectra showed clear differences between whole wheat flour (WWF) and its acid hydrolysate (WWFH). The native WWF displayed broad, flat absorptions across 4000 to 500 cm^{-1}, which is typical of intact starch, cellulose, and protein macromolecules, whereas hydrolysis sharpened and intensified the O–H stretching band at 3200 to 3600 cm^{-1}, indicating hydrogen-bond cleavage and exposure of free hydroxyls; the methylene C–H band near 2900 cm^{-1} weakened, confirming carbohydrate backbone breakdown, and reduced intensities at 1644 cm^{-1} (amide I) and 1404 cm^{-1} (C–H bend) pointed to protein degradation. Strong new peaks at 1000 to 1200 cm^{-1} (C–O–C and C–O stretching) reflected conversion of inert biopolymers into reactive small-molecule phenolics and sugars. The small-molecule phenolics detected in the WWFH spectrum are attributed to the partial degradation of lignin present in the whole wheat flour (typically 1 to 2 wt %) under acid hydrolysis conditions, which releases phenolic compounds such as phenolic acids and aldehydes. Additionally, tyrosine residues from protein degradation may also contribute to the phenolic hydroxyl signals. Compared with neat UF, WFUF retained the same overall peak positions, so the basic UF skeleton stayed intact, yet the 3319 cm^{-1} band (–NH/–OH) grew stronger and broader while the 2960 cm^{-1} methylene peak intensified, signaling more active groups and additional methylene crosslinks. Peaks at 1630 cm^{-1} (C=O) and 1534 cm^{-1} (amide II N–H) increased slightly and shifted, suggesting hydrolysate groups entered the cure reaction, and enhanced absorptions at 1241 cm^{-1} (C–N/C–O) and 1012 cm^{-1} (hydroxymethyl/ether) indicated more stable ether crosslinks (Gao *et al*. 2020; Ma *et al*. 2022; Xu *et al*. 2022; Li *et al*. 2023). These changes confirm that WWFH components were chemically incorporated (Gao *et al*. 2020; Ma *et al*. 2022; Li *et al*. 2023) rather than simply physically mixed, producing a denser, more stable network. The possible chemical reactions between WWFH and UF resin *via* dehydration condensation are schematically presented in Fig. S1 (Supporting Information).

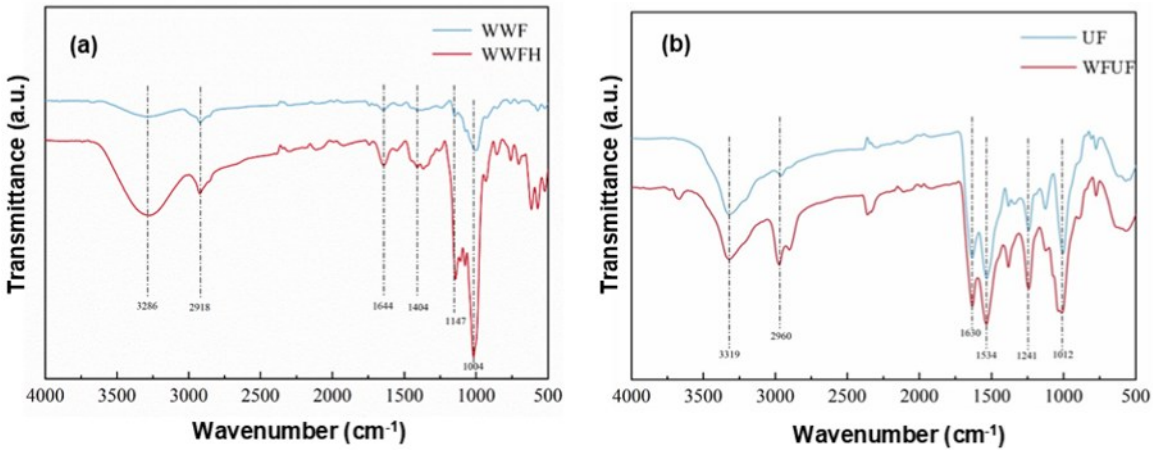

Fig. 4. FT-IR spectra: (a) WWF and WWFH; (b) UF resin and WFUF

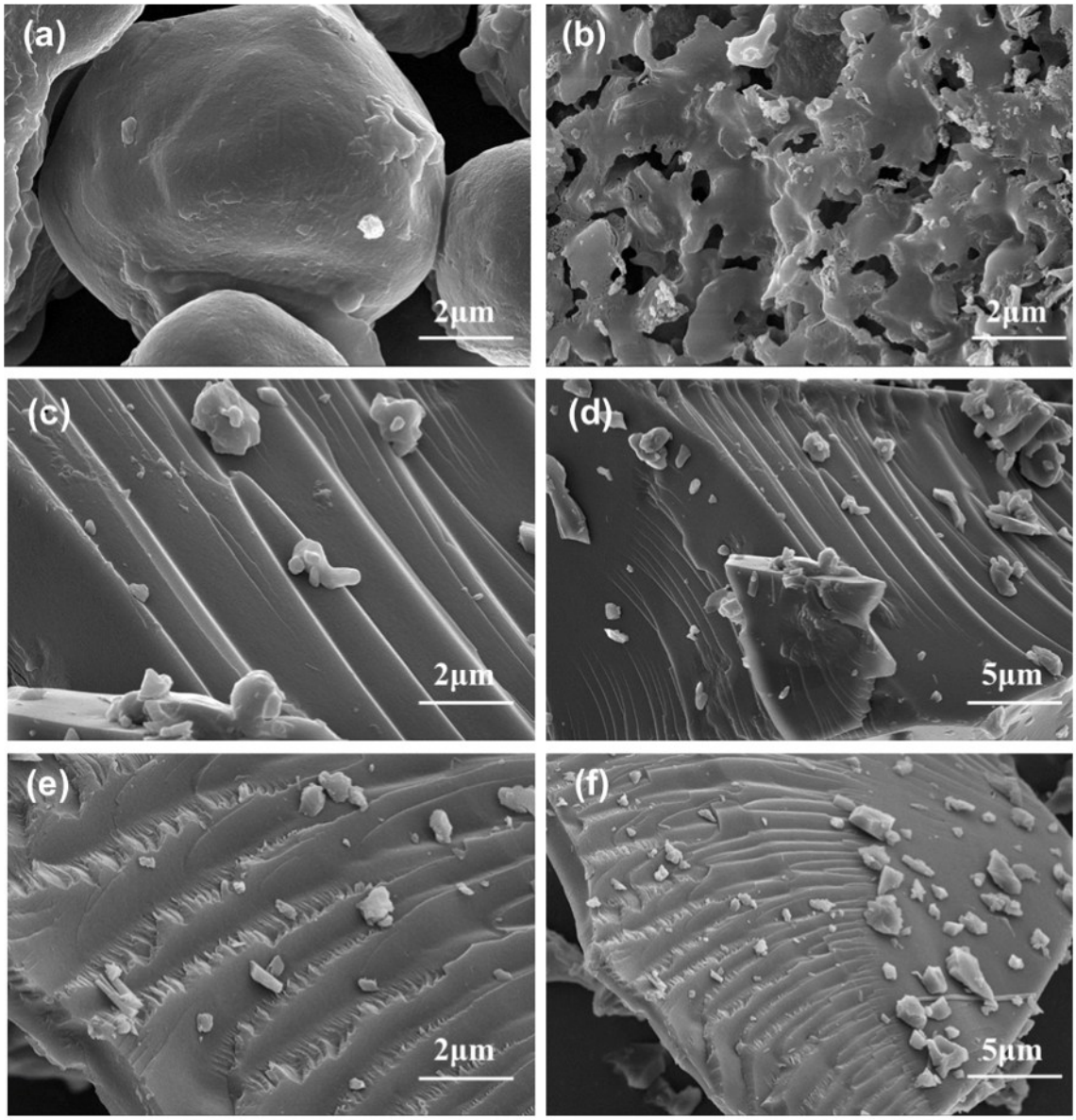

Fig. 5. SEM images of (a) WWF, (b) WWFH, (c,d) UF resin, and (e,f) WFUF resin

Morphology

SEM observation was carried out to compare the fracture micromorphology of cured pure UF and WF adhesives, as well as raw flour and hydrolysate. As shown in Fig. 5, raw WWF appeared as smooth, spherical granules with dense, intact surfaces and almost no visible pores. Acid hydrolysis destroyed this ordered structure, producing a honeycomb-like porous network riddled with cracks and fragmented crosslinks. The markedly increased surface area exposed abundant reactive sites for subsequent crosslinking with the aldehyde resin. Pure UF resin showed a smooth, flat fracture surface with continuous, straight, layered crack patterns and only scattered fine debris (Yang *et al*. 2023; Dukarska *et al*. 2024; Psochia *et al*. 2025). This planar morphology reflects classic brittle fracture in thermosets.

The rigid, uniform network inside neat UF allows cracks to propagate rapidly along fixed paths with little energy dissipation, which explains its poor toughness, low impact resistance, and tendency to crack under stress. WFUF resin exhibited a rough, uneven fracture surface with disordered, tortuous crack paths and extensive folded textures. The biomass components were uniformly embedded in the matrix with tight interfacial bonding.

This rugged morphology indicates ductile fracture. The tortuous crack path lengthens the total propagation distance, while simultaneous microcracking, interfacial debonding, and matrix tearing absorb substantial impact energy. Crack tips are effectively blunted, preventing rapid unstable growth and improving overall resistance to damage. These changes stem from the chemical participation of bio-based modifiers in curing. Hydrolyzed WWF interacts with UF prepolymers to enhance interfacial compatibility (Yang *et al*. 2023; Dukarska *et al*. 2024). The interaction results in reduced defects and voids, toughening of the rigid network, and release of internal shrinkage stresses generated during curing.

TG-DTG

TG-DTG tests were conducted to investigate the thermal decomposition characteristics of cured UF and WFUF resin samples. Thermo-gravimetry (TG) and derivative thermogravimetry (DTG) curves in Fig. 6 compare the thermal behavior (Gao *et al*. 2020; Antov *et al*. 2021; Ma *et al*. 2022; Tian *et al*. 2023) of neat UF and WFUF resins. Both samples degraded in three stages. From room temperature to 200 °C, minor weight loss from moisture, and volatile oligomers were comparable. Between 200 and 400 °C, the main decomposition of methylene bridges and hydroxymethyl crosslinks occurred. WFUF consistently retained more mass than UF in this range, indicating improved thermal stability. Beyond 400 °C, organic components were fully degraded and residual char stabilized at similar levels for both resins.

The DTG curve of neat UF showed a sharp, intense peak between 200 and 300 °C, reflecting rapid concentrated decomposition. For WFUF, the main peak shifted to higher temperature, its intensity decreased, and the profile broadened. A shoulder peak near 200 °C also appeared. These changes indicate that WWFH polysaccharides and active groups reacted with the UF prepolymer to build a denser three-dimensional crosslinked network (Ma *et al*. 2022; Tian *et al*. 2023), while the shoulder reflects stepwise thermal degradation of biomass components. Overall, WWFH modification was found to improve the UF network, slow thermal breakdown, and achieve improved thermal stability.

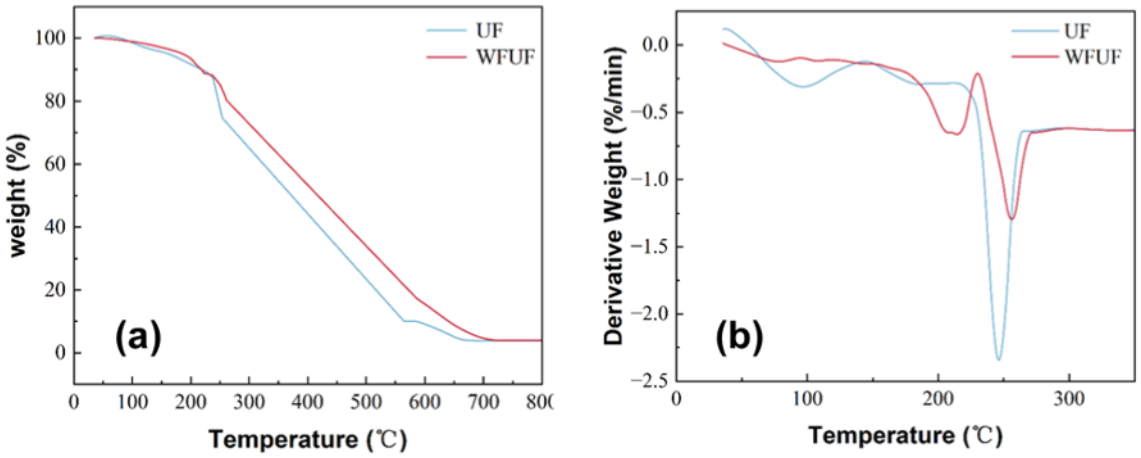

Fig. 6. TG-DTG plots of UF and WFUF: (a) TG of UF and WFUF; (b) DTG of UF and WFUF

Future Work

Overall, this work elucidated the multi-component cross-linking interaction mechanism of whole wheat flour hydrolysate (WWFH) modified urea-formaldehyde (WFUF) resin and optimized its co-polycondensation process, providing support for high-value utilization of low-value industrial-grade whole wheat flour and development of high-performance bio-based wood adhesives. Future work will focus on addressing the slight increase in formaldehyde emission, quantifying the crosslinking mechanism, and verifying industrial application potential (Wibowo and Park 2024; Xu *et al*. 2024; Zhang *et al*. 2025). The key research directions are as follows:

1. Investigate the curing kinetics of WFUF resin *via* differential scanning calorimetry (DSC) and systematically examine the effects of hydrolysis degree on resin microstructure and properties to clarify the precise structure-activity relationship.
2. Quantify the competitive formaldehyde capture mechanism of protein and reducing sugar components in WWFH.
3. Evaluate the long-term aging and cyclic wet-dry resistance of plywood.

CONCLUSIONS

1. Under the optimized co-polycondensation conditions (F/U molar ratio of 1.2, whole wheat flour hydrolysate (WWFH) viscosity of 31 to 40 s, and hydrolysate addition amount of 15%), the wet bonding strength of wheat flour-based urea-formaldehyde (WFUF) resin reached 1.30 MPa, which represented a 54.8% increase compared to pure UF resin, while the dry bonding strength remained comparable. The formaldehyde emission of WFUF resin was 0.59 mg/L, which still satisfied the E1 GB 18580 (2017) grade environmental standard.
2. Fourier transform infrared (FTIR) spectrometry, scanning electron microscopy (SEM), and thermogravimetric (TG) characterizations confirmed that WWFH was not simply physically blended with the UF matrix. The reducing sugars, protein degradation products, and pentosan components in WWFH formed multiple crosslinking structures

with UF resin, reducing crystallinity, increasing crosslinking density, and significantly improving the resin's thermal stability and toughness.

ACKNOWLEDGMENTS

This research was funded by the Guangxi Innovation-Driven Development Project (31360581, AA18118044, AA17204067), China; National Natural Science Foundation of China, China.

Conflict of Interest

The authors declare that they have no known competing financial interests or personal relationships that could have appeared to influence the work reported in this paper.

Use of Generative AI

The author used a large language model (DeepSeek) for language translation and text polishing. After using this tool, the author reviewed and edited the content as needed and take full responsibility for the content of the publication.

REFERENCES CITED

Antov, P., Savov, V., Krišťák, Ľ., Réh, R., and Mantanis, G. I. (2021). "Eco-friendly, high-density fiberboards bonded with urea-formaldehyde and ammonium lignosulfonate," *Polymers* 13(2), article 220. https://doi.org/10.3390/polym13020220

Calvez, I., Garcia, R., Koubaa, A., Landry, V., and Cloutier, A. (2024). "Recent advances in bio-based adhesives and formaldehyde-free technologies for wood-based panel manufacturing," *Current Forestry Reports* 10, 386-400. https://doi.org/10.1007/s40725-024-00227-3

Dhawale, P. V., Vineeth, S. K., Gadhave, R. V., Fatima, J. M. J., Supekar, M. V., Thakur, V. K., and Raghavan, P. (2022). "Tannin as a renewable raw material for adhesive applications: A review," *Materials Advances* 3, 3365-3388. https://doi.org/10.1039/D1MA00841B

Dorieh, A., Selakjani, P. P., Shahavi, M. H., Pizzi, A., Movahed, S. G., Pour, M. F., and Aghaei, R. (2022). "Recent developments in the performance of micro/nanoparticle-modified urea-formaldehyde resins used as wood-based composite binders: A review," *International Journal of Adhesion and Adhesives* 114, article 103106. https://doi.org/10.1016/j.ijadhadh.2022.103106

Dukarska, D., Kawalerczyk, J., and Kmieciak, J. (2024). "Modified pine needles as a formaldehyde scavenger for urea-formaldehyde resin in plywood production," *European Journal of Wood and Wood Products* 82, 147-158. https://doi.org/10.1007/s00107-023-01998-5

Dunky, M. (1998). "Urea-formaldehyde adhesive resins for wood," *International Journal of Adhesion and Adhesives* 18(2), 95-107. https://doi.org/10.1016/S0143-7496(97)00054-7

Fritz, C., and Olivera, J. F. (2022). "Nanocellulose in heterogeneous water-based polymerization for wood adhesives," *Polysaccharides* 3(1), 219-235. https://doi.org/10.3390/polysaccharides3010012

Gao, S., Liu, Y., Wang, C., Chu, F., Xu, F., and Zhang, D. (2020). "Synthesis of lignin-based polyacid catalyst and its utilization to improve water resistance of urea-formaldehyde resins," *Polymers* 12(1), article 175. https://doi.org/10.3390/polym12010175

GB 18580-2017 (2017). "Indoor decorating and refurbishing materials - Limit of formaldehyde emission of wood-based panels and finishing products," Standardization Administration of China, Beijing, China.

GB/T 14074-2017 (2017). "Testing methods for wood adhesives and their resins," Standardization Administration of China, Beijing, China.

GB/T 1723-1993 (1993). "Determination of viscosity of coatings," Standardization Administration of China, Beijing, China.

GB/T 17657-2022 (2022). "Test methods of evaluating the properties of wood-based panels and surface decorated wood-based panels," Standardization Administration of China, Beijing, China.

Hussin, M. H., Abd Latif, N. H., Hamidon, T. S., Idris, N. N., Hashim, R., Appaturi, J. N., Brosse, N., Ziegler-Devin, I., and Chrusiel, L. (2022). "Latest advancements in high-performance bio-based wood adhesives: A critical review," *Journal of Materials Research and Technology* 21, 3909-3946. https://doi.org/10.1016/j.jmrt.2022.10.156

Kawalerczyk, J., Dziurka, D., Mirski, R., and Trociński, A. (2019). "Flour fillers with urea-formaldehyde resin in plywood," *BioResources* 14(3), 6727-6735. https://doi.org/10.15376/biores.14.3.6727-6735

Khorramabadi, L. A., Behrooz, R., and Kazemi, S. (2023). "Effects of nanoclay modification with aminopropyltriethoxysilane on the performance of urea-formaldehyde resin adhesives," *BioResources* 18(3), 5417-5434. https://doi.org/10.15376/biores.18.3.5417-5434

Kong, X., Wei, Z., Xia, S., Jia, B., Gan, L., and Han, S. (2023). "The characterizations of nanofluid type urea formaldehyde resins," *International Journal of Adhesion and Adhesives* 125, article 103416. https://doi.org/10.1016/j.ijadhadh.2023.103416

Kumar, C., and Leggate, W. (2022). "An overview of bio-adhesives for engineered wood products," *International Journal of Adhesion and Adhesives* 118, article 103187. https://doi.org/10.1016/j.ijadhadh.2022.103187

Li, D., Yu, L., Li, L., Liang, J., Wu, Z., Xu, X., Zhong, X., and Gong, F. (2023). "Melamine-urea-formaldehyde resin adhesive modified with recycling lignin: Preparation, structures and properties," *Forests* 14(8), article 1625. https://doi.org/10.3390/f14081625

Liu, K., Su, C., Ma, W., Li, H., Zeng, Z., and Li, L. (2020). "Free formaldehyde reduction in urea-formaldehyde resin adhesive: Modifier addition effect and physicochemical property characterization," *BioResources* 15(2), 2339-2355. https://doi.org/10.15376/biores.15.2.2339-2355

Hogger, E. M., Van Herwijnen, H. W. G., Moser, J., Kantner, W., and Konnerth, J. (2021). "Systematic assessment of wheat extenders in formaldehyde-condensation plywood resins: Part II – Mechanical properties of plywood panels," *The Journal of Adhesion* 97(14), 1310-1321. https://doi.org/10.1080/00218464.2020.1756788

Ma, Y., Luo, Y., Zhang, Q., Gao, Y., Li, J., Shah, S., Wang, X., and Zhang, X. (2022). "Biodegradable films prepared from pulp lignocellulose adhesives of urea formaldehyde resin modified by biosulfonate," *Polymers* 14(14), article 2863. https://doi.org/10.3390/polym14142863

Moutousidis, D., Karidi, K., Athanasiadou, E., Stylianou, E., Giannakis, N., and Koutinas, A. (2023). "Reinforcing urea-formaldehyde resins with pectins derived from orange peel residues for the production of wood-based panels," *Sustainable Chemistry for the Environment* 4, article 100037. https://doi.org/10.1016/j.scenv.2023.100037

Park, S., and Park, B.-D. (2021). "Crystallinity of low molar ratio urea-formaldehyde resins modified with cellulose nanomaterials," *Journal of the Korean Wood Science and Technology* 49(2), 169-180. https://doi.org/10.5658/WOOD.2021.49.2.169

Pu, H., Han, K., Dai, R., and Shan, Z. (2022). "Semi-liquefied bamboo modified urea-formaldehyde resin to synthesize composite adhesives," *International Journal of Adhesion and Adhesives* 113, article 103061. https://doi.org/10.1016/j.ijadhadh.2021.103061

Saito, K., Hirabayashi, Y., and Yamanaka, S. (2021). "Reduction of formaldehyde emission from urea-formaldehyde resin with a small quantity of graphene oxide," *RSC Advances* 11, 32830-32836. https://doi.org/10.1039/D1RA06717F

Sandahl, A., Pedersen, L. S., Taarning, E., and Lindhardt, A. (2022). "Evaluation of glycolaldehyde as a formaldehyde substitute in urea-based wood adhesives," *BioResources* 17(4), 5769-5784. https://doi.org/10.15376/biores.17.4.5769-5784

Shao, J., Chen, Y., Dong, L., Yuan, T., Zhang, Z., and Zhang, J. (2022). "Correlation between the desiccator method and 1 m³ climate chamber method for measuring formaldehyde emissions from veneered particleboard," *Processes* 10(5), article 1023. https://doi.org/10.3390/pr10051023

Song, S., Liu, J., Feng, R., Wu, C., Peng, W., and Gan, W. (2025). "Research on the development of modified adhesives based on the phenol liquefaction products of bagasse pulp concentrate black liquor." *Industrial Crops & Products* 230, article 121112. https://doi.org/10.1016/j.indcrop.2025.121112

Wang, H., Liang, J., Zhang, J., Zhou, X., and Du, G. (2017). "Performance of urea-formaldehyde adhesive with oxidized cassava starch," *BioResources* 12(4), 7590-7600. https://doi.org/10.15376/biores.12.4.7590-7600

Wibowo, E. S., and Park, B.-D. (2024). "Effects of wheat flour levels on the thermal curing behavior of urea-formaldehyde and phenol-formaldehyde resins," *International Journal of Adhesion and Adhesives* 132, article 103694. https://doi.org/10.1016/j.ijadhadh.2024.103694

Xu, G., Tian, H., Xi, X., Song, J., Lei, H., and Du, G. (2022). "Preparation and characterization of urea-formaldehyde adhesives modified with glyoxalated tannin," *European Journal of Wood and Wood Products* 80, 1131-1143. https://doi.org/10.1007/s00107-022-01819-1

Xu, Y., Zhang, Q., Lei, H., Zhou, X., Zhou, X., Zhao, D., Du, G., Pizzi, A., and Xi, X. (2024). "A formaldehyde-free amino resin alternative to urea-formaldehyde adhesives: A bio-based oxidized glucose-urea resin," *Industrial Crops and Products* 218, article 119037. https://doi.org/10.1016/j.indcrop.2024.119037

Yang, P., Zhu, Z., Wang, L., Shen, A., Tang, M., Chen, M., Cao, Y., Dai, H., and Zhou, X. (2023). "Developing carbon dots as green modifiers for improving the bonding performance of low-molar-ratio urea-formaldehyde resin," *International Journal of Adhesion and Adhesives* 125, article 103416. https://doi.org/10.1016/j.ijadhadh.2023.103416

Zhang, B., Huang, S., and Wang, X. (2025). "Hydrochar derived from sugarcane bagasse as a full replacement for wheat flour filler in urea-formaldehyde adhesives for plywood," *Results in Engineering* 26, article 106569. https://doi.org/10.1016/j.rineng.2025.106569

Article submitted: May 19, 2026; Peer review completed: August 15, 2026; Revised version received and accepted: September 13, 2026; Published: October 13, 2026.
DOI: 10.15376/biores.21.4.11562-11580

APPENDIX

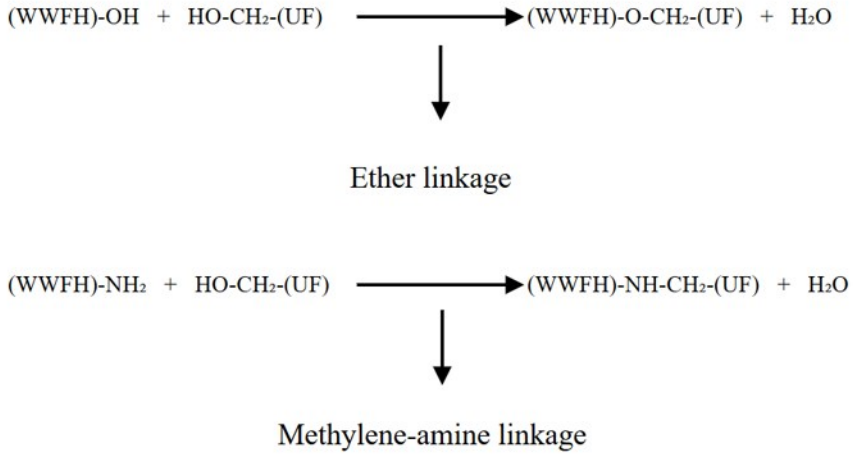

Fig. S1. Possible chemical reactions between WWFH and UF resin

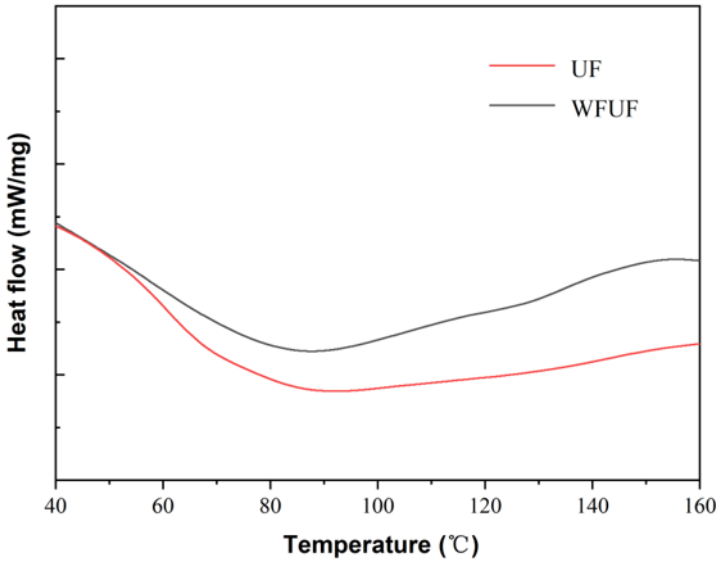

Fig. S2. DSC curves of UF resin and WFUF resin

Table A1. UF Resin and WFUF Resin XPS Test Data

Sample	C1s			N1s			O1s		
	Binding Energy	FWHM	Atomic Percentage	Binding Energy	FWHM	Atomic Percentage	Binding Energy	FWHM	Atomic Percentage
	(eV)	(eV)	(%)	(eV)	(eV)	(%)	(eV)	(eV)	(%)
UF	284.97	2.8	70.38	399.18	1.41	18.17	531.31	1.87	11.45
WFUF	285.02	2.66	73.78	399.37	1.55	12.03	532.45	2.21	13.92

Table A2. UF Resin and WFUF Resin XPS C1 Signal Detection Data

Sample	Binding Energy (eV)				Atomic Percentage (%)			
	C-C	C-O	O-C-O	C=O	C-C	C-O	O-C-O	C=O
UF	284.8	286.28	287.29	288.86	30.55	11.45	18.22	27.17
WFUF	284.8	286.08	287.29	288.29	25.83	26.98	20.39	24.77

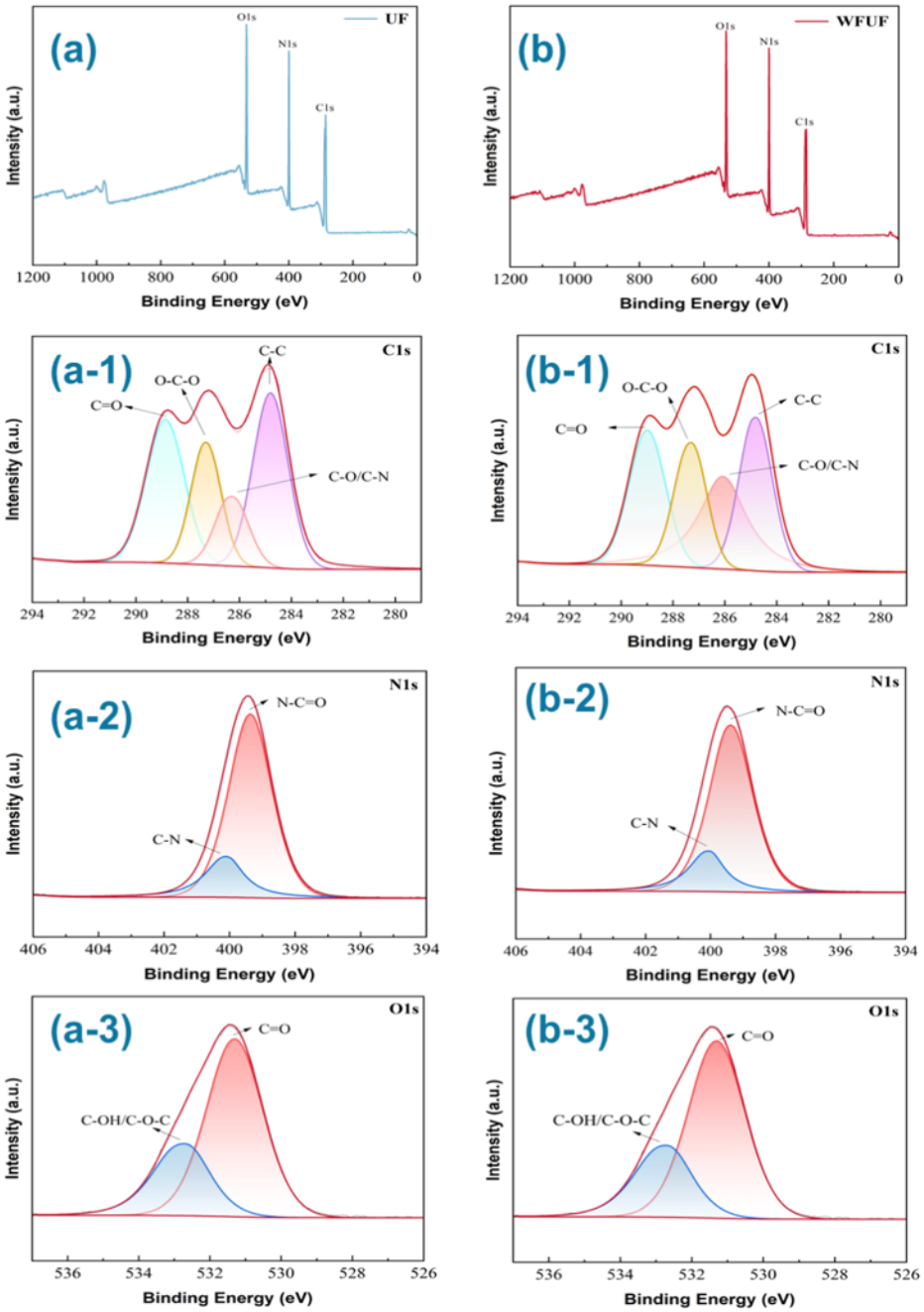

Fig. S3. XPS plots of UF resin (a) and WFUF resin (b)